GSA Data Repository 2017162

Alexander J. Horton, José Antonio Constantine, Tristram C. Hales, Benoît Goossens, Michael W. Bruford, and Eli D. Lazarus, 2017, Modification of river meandering by tropical deforestation: Geology, doi:10.1130/G38740.1

Text DR1. Methods

Discharge data recorded at Balat (1978 – 2013) (**Fig. DR1)** and Barik Menis (2000 – 2013) gauging stations (**Fig. 1** of manuscript) were provided by the Department of Irrigation and Drainage in Kota Kinabalu, Sabah, Malaysia. Bankfull discharges (Q_b) were estimated fitting a type-two Gumbel distribution to annual maxima data from the Balat gauging station, the more complete of the two data sets. We assume Q_b corresponds to the 1.5 year recurrence event (Dury, 1976; Castro and Jackson, 2001). Without sufficient annual maxima data from the Barik Menis gauging station to repeat this process there, the bankfull estimate at Balat gauging station was adjusted based on the ratio of average daily flow between the two gauging stations, and the increase between the two assumed to be linearly proportional to streamwise distance. The estimate of Q_b at Balat was then adjusted for each study reach based on the streamwise distance between the study reach and Balat.

Average longitudinal water-surface slope (S) for each meander was estimated using the Manning formula:

$$U = \frac{R^{\frac{2}{3}}}{n} S^{\frac{1}{2}} \qquad \text{(S2)}$$

where R is the hydraulic radius, and n is the manning's roughness coefficient, here taken as 0.035 (Coon, 1997). These values are consistent with estimates of valley slope derived from SRTM digital elevation data for the region.

Reach averaged bankfull depths (h) for reaches C and D were taken from measured channel cross-sections, where bankfull stage was assumed to be the level at which vegetation ceased to grow on the point bar. Cross-sections were measured using a sonic depth gauge (Norcross Hawkeye H22PX) when the river was at or very near bankfull flow conditions. Access to reaches A and B was

restricted, therefore a representative width to depth ratio was calculated from reaches C and D, and used to estimate bankfull depths for reaches A and B.

The scour factor (A) was determined from cross section data for reaches C and D using the equation:

$$A = -\frac{m}{hnc} \quad \text{(S1)}$$

where n is the cross-stream coordinate, m is the local bed elevation, h is bankfull depth, and c is local curvature (Constantine et al., 2009). At the channel centre, both n and m are 0. To better represent the secondary flow induced by the imbalance between the lateral pressure gradient and centripetal force, we modify the scour factor according to Johannesson and Parker (1989).

Curvature was calculated at a spacing of 200 m along each centreline so as to capture the arc of the meander without being influenced by small-scale local variations. Curvature values were found by fitting a circle of radius r (units m) to three successive points along a river centreline (s_{i-1}, s_i, and s_{i+1}) such that all three points sit on the circle's circumference, with a curvature value of $\frac{1}{r}$ being assigned to the middle point s_i. This was achieved by providing an initial estimate for the center point of the circle ($\bar{s}$) and using a sequential least squares optimising algorithm (Kraft, 1988) to reduce the error in the difference between the distances from the estimated centre point to each of the three points (s_{i-1}, s_i, and s_{i+1}) to below 0.01 m. This optimised centre point yields three estimates of r, of which we used the mean to define curvature (c) at point s_i (**Fig. DR2**). We report the maximum values of curvature for each river section.

Likewise, values of the velocity perturbation we report are taken as the maximum value within each river section, constituting a conservative estimate for the corresponding erodibility coefficient.

The automated process of identifying riverbank position from each Landsat derived NDVI mosaic resulted in a polygon outlining the river's extent in each of the four study reaches. These

polygons were then used to estimate reach averaged bankfull widths (*2b*) by dividing the area of each by the length of the corresponding river centreline (**Table. DR1**).

Characteristic rooting depths for forested and cleared sections of the river were estimated by digging trial pits at 9 different locations, and from field observations of root structure within exposed cut banks. Along forested sections of the river the trial pits revealed a densely intertwined root network at the surface, comprised mainly of fine roots, but encompassing a wide range of diameters. Fine roots were largely confined to the top 0.5 m, below which the average diameter increased with depth, while the root density rapidly declined. At the maximum trial pit depths of 1.0–1.5 m, nearly all roots were absent, with the exception of a few with the largest diameters (> 15 mm). Observations of exposed cut banks along forested sections suggest that these larger roots tend not to extend below ~2 m.

Cleared sections of riverbank were almost exclusively colonized by grass species (*Phragmites australis* and *Pennisetum purpureum*), whose root structure was located below clumped stands of stems distributed 0.5–1 m apart. This meant that root density was very heterogeneous, with regions between stands where roots were sparse. Below the stem stands, roots formed a top-heavy conical structure with a large tap root extending downwards to ~0.5 m and with many fine roots extending latterly at the surface, reducing in density with depth. At the bottom of trial pits (~1.0 m) only trace amounts of fine roots were found.

To distinguish between forested river sections, and those cleared of forest, we developed a land classification scheme using the software eCognition, which uses a set of training data to identify spectral signatures and shape parameters (Baatz et al., 2000) from the 2009 Landsat 5 set of bandwidths that correspond to forested land, agricultural land, and bare earth. The set of training data were constrained to areas that were clearly visible in a high-resolution image (Google Earth™), and to areas that we had observed in the field. To verify this classification scheme, we applied it to the remainder of the 2009 Landsat image and confirmed its application using Google Earth™. We then applied this classification to each Landsat image prior to 2009 to identify sections along the river that

underwent forest clearing. Forested river sections in the 2014 Landsat 8 image were identified using several high resolution images from Google Earth™.

Field observations of the Kinabatangan River along reaches C and D (Fig. 1 of manuscript) show it to be sand-bedded, although we were unable to obtain samples of bed material to determine characteristic grain size.

Text DR2. Uncertainty

To assess the error inherent in our measurements of meander migration, we identified 17 river sections located through reaches B and C where high resolution (60cm pixel size) DigitalGlobe™ imagery was available for the years 2009 and 2014 via Google Earth™. By delineating bank lines from these high resolution images, and measuring the migration of the river centerline, we compared these results with those obtained from Landsat imagery for the same time span. The mean absolute difference in the centreline migrations derived from these two sources is 1.46 m ($\sigma = 1.12$), which, when averaged over the timespan of 5 years, provides an estimate for error in our measurement of meander migration rates of 0.29 m/yr. While we acknowledge that there is still error in the use of high resolution imagery to measure meander migration, the error associated with measurements taken from images with 60 cm resolution will be insignificant compared to those taken from images with 30 m resolution. (Due to the lack of available images spanning our study reaches, we were unable to extend the range of high resolution meander migration measurements.)

REFERENCES CITED

Baatz, M., Schäpe, A., Strobl, J., Blaschke, T., and Griesebner, G., 2000, Multiresolution Segmentation-an optimization approach for high quality multi-scale image segmentation: Angewandte Geographische Informationsverarbeitung, v. 12, p. 12–23.

Coon, W. F., 1997, Estimation of roughness coefficients for natural stream channels with vegetated banks: USGS Water-Supply Paper, v. 2441, p. 1–133.

Kraft, D. A., 1988, software package for sequential quadratic programming: DFVLR Obersfaffeuhofen, Germany.

Table DR1: Reach measurements of river area, centreline length and corresponding average widths for each Landsat image.

	Reach A			Reach B			Reach C + D			Total		
Year	Area	Length	Width	Area	Length	Width	Area	Length	Width	Area	Length	Width
1989	4784320	54400	87.95	4889936	43300	112.93	6680857	49600	134.69	16355113	147300	111.03
1996	4774540	54400	87.78	4969936	43400	114.49	6666429	49800	133.86	16410905	147600	111.19
2001	5003576	54400	91.98	4919638	43400	113.38	7013878	49900	140.56	16937093	147700	114.68
2005	4834398	54500	88.70	4854038	43500	111.59	7027178	50100	140.27	16715614	148100	112.87
2009	5042701	54500	92.53	5037636	43500	115.82	6772678	50300	134.64	16853015	148300	113.64
2014	4759049	54500	87.32	5020536	43600	115.14	6990878	50500	138.43	16770463	148600	112.85
Average Width			89.38			113.89			137.08			112.71

102 Table DR2. Values used in calculation of ω

River Section:	Reach A (1 – 20)	Reach B (21 – 40)	Reach C (41 – 56)	Reach D (57 – 67)
Bankfull discharge Q_b [m^3 / s]	947.86	1242.27 (1428.61 after tributary)	1708.42	2198.64
Average bankfull width *2b* [m]	89.38	113.89	130.16	146.23
Average bankfull depth *h* [m]	5.2	6.7	7.83	8.33
Average Slope *S*	0.0004	0.0003	0.0003	0.0003
Manning's roughness coefficient *n*	0.035	0.035	0.035	0.035
Scour Factor *A*	3	3	3	3

103

104

105 Table DR3. List of reach characteristics

	Reach A (Section 1 – 20)	Reach B (Section 21 – 40)	Reach C (Section 41 – 56)	Reach D (Section 57 – 67)
Streamwise length [m]	54500	43603	29415	21088
Sinuosity	2.73	2.41	1.46	2.64
Upstream Coordinates [^{0}lat, ^{0}lon]	5.2217, 117.4982	5.3595, 117.6655	5.4123, 117.9394	5.4106, 118.0789
Downstream Coordinates [^{0}lat, ^{0}lon]	5.3595, 117.6655	5.4729, 117.7989	5.4106, 118.0789	5.4600, 118.1573
No. cleared river sections	7	6	4	5

106

107

Table DR4. Landsat image identification

Year	Path	Row	ID
1989	117	056	LT51170561989264BKT00
1996	117	056	LT51170561996220CLT00
2001	117	056	LE71170562001177EDC00
2005	117	056	LT51170562005260BKT00
2009	117	056	LT51170562009223BKT00
2014	117	056	LC81170562014365LGN00

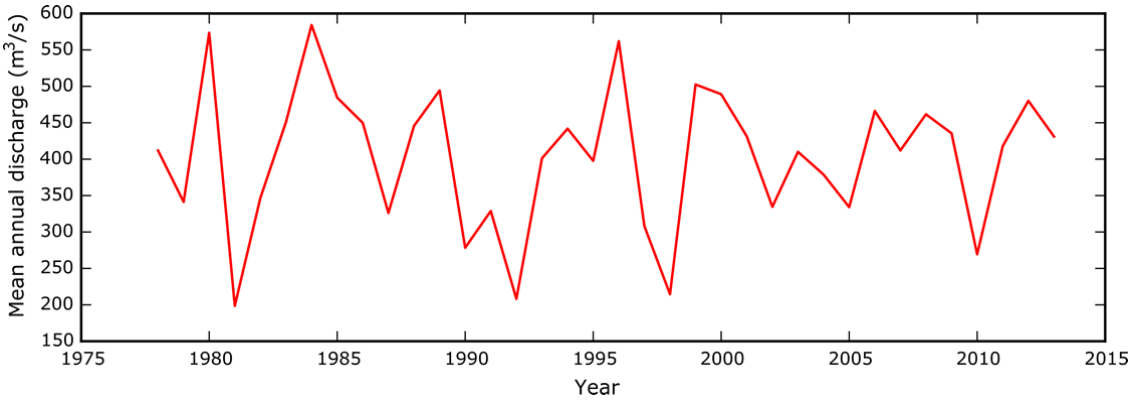

Figure DR1: Mean annual discharge data collected from Balat gauging station (1978 – 2013).

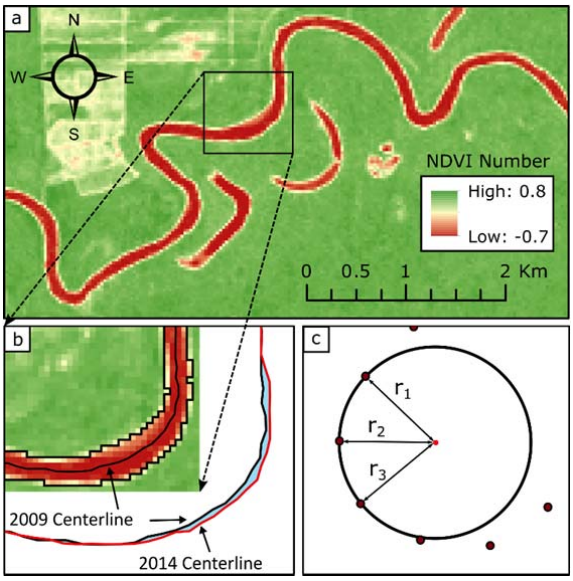

Figure DR2. Meander migration and curvature calculation methodologies. **a**, NDVI mosaic derived from TM/Landsat-5 image (11/10/2009). **b**, Automatically derived river bank lines and associated river centreline for 2009 image, 2009 and 2014 centrelines superposed to form a polygon representing the area eroded. **c**, Fitting of circle to estimate curvature ($\frac{\mathbf{1}}{\bar{r}}$) at point r_2.

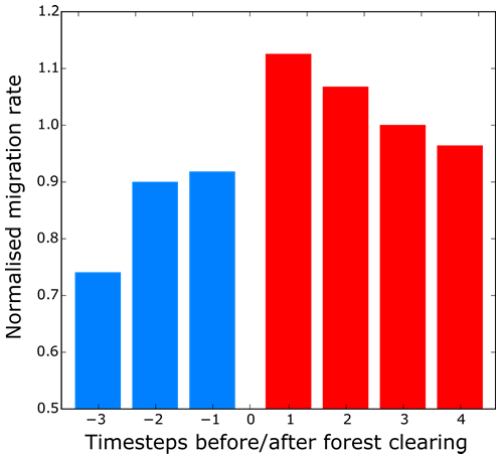

Figure DR3: Mean migration rates for sections of river that have been cleared of forest, sorted by the number of time steps (successive pair of Landsat images i.e., 1989-1996, 1996-2001, 2001-2005, 2005-2009, 2009-2014) before and after forest clearing. Migration rates for individual river sections have been normalised by the mean migration rate across all time steps for that river section.